EUSIPCO 2013 1569744049

FIBER SENSING USING UFWT-LASERS AND SPARSE ACQUISITION

Christian Weiss *Abdelhak M. Zoubir*

Signal Processing Group
Technische Universität Darmstadt
64283 Darmstadt, Germany
E-mail: {cweiss, zoubir}@spg.tu-darmstadt.de

ABSTRACT

We propose a sparse acquisition technique for fiber Bragg grating (FBG) sensors with subsequent sparse reconstruction and provide an analytical model for the received sensing signal. High sampling rates require expensive hardware components such as A/D converters or filters which are replaced by a compressive sensing scheme to abate the sampling rate far below Nyquist which may also lower the system costs. Moreover, storage requirements are strongly reduced. Our proposed scheme exploits the characteristics and sparse structure of the reflected signal for which a detailed model is presented.

Index Terms— Fiber Bragg grating sensor, wavelength-tunable lasers, mode-locked fiber lasers, compressive sensing

1. INTRODUCTION

Fiber Bragg-Grating (FBG) sensors continue to gain more importance over the last years [1, 2, 3, 4, 5]. Owing to their versatile structure, they provide highly desirable features as compared to electrical sensors such as lightweight, small size, wide bandwidth, resistance against electro-magnetic interference and environmental ruggedness [6]. FBGs exhibit high sensitivity to different impairments, e.g. strain or temperature, which have been extensively studied in the past [2]. They have been applied in a variety of applications ranging from distributed sensing for structural monitoring [2, 3] over chemical sensing [7] and medical applications such as optical coherence tomography [8] or wearable sensors for ubiquitous health monitoring [4].

Sensors deploying a broadband light source for simultaneous observation at all wavelengths suffer from a low local signal-to-noise ratio (SNR) which motivates the use of ultra-fast wideband wavelength-tunable (UFWT) fiber lasers. The authors in [3, 9] presented a new type of UFWT lasers based on active mode-locking and dispersion tuning without the need of any tunable filters which reduces hardware costs and allows for very high sweep rates required for dynamic sensing. The application of UFWT lasers to FBG sensing showed excellent results in terms of sweep range and scan speed superior to other existing FBG sensor systems [3, 9]. Due to this fact, we consider a signal model based on this class of laser sources as presented in [3, 9]. However, fast sweep rates require high sampling rates and produce vast data which increases the hardware costs of an automated sensing and detection system. Such problems can be tackled efficiently by compressive sensing (CS) [10].

Our novel approach to FBG sensing aims to exploit the advantages of both, UFWT lasers according to [3, 9] and CS-based acquisition. Practical verification is provided using experimental data acquired from the original system in [3, 9].

This paper is organized as follows. In Section 2, we present the modified system setup for CS-based FBG sensing using UFWT-lasers. A comprehensive signal model for the reflected signal is provided in Section 3, while the application of CS to FBG sensing is explained in Section 4. In Section 5, we show simulations and experimental verification before concluding this work in Section 6.

2. FBG SENSOR SYSTEM

An FBG sensing system combined with CS has various desirable features such as fast sweep rates, wide sweep ranges and high spatial resolution at low sampling rates in addition to small storage and hardware costs. We consider the fiber sensing system depicted in Figure 1, aiming to address these requirements. It deploys an UFWT-class laser and is based on the experimental setup in [3, 9] which has been extended by a CS-based acquisition module. A semiconductor optical amplifier (SOA) acts as gain medium for the UFWT-laser. Using an external intensity modulator, the injection current of the SOA is directly modulated by a sine-signal in order to achieve a pulsed output via active mode-locking [3, 9]. The authors in [3, 9] propose dispersion tuning to linearly sweep through the lasing wavelength, where the falling edge of a triangular waveform is applied to modulate the frequency f_m of the SOA-modulating signal. No tunable filters are needed which allows for fast sweep rates and reduced hardware costs. A dispersion compensating fiber (DCF) forms a highly dispersive laser cavity in which mode-locking is only possible within a small spectral range around a center wavelength. When the frequency of the modulating signal is changed, the center las-

ing wavelength is swept along the SOA gain bandwidth and pulses at different wavelenghts are constantly generated. Frequency and wavelength changes show a linear dependence. The tuning sensitivity is measured in wavelength shift per Hz of change in the modulation frequency (nm/Hz) [3, 9].

We assume a scaling of the optical power introduced into the sensing fiber such that non-linear effects can be neglected. The FBGs represent the sensing points of the system. Each of their reflectivity spectra is shifted with respect to the others by detuning. As in [3, 9], we choose FBG$_j, j \in \{1, ..., K\}$ as a reference point which is never subject to any kind of perturbation and we call the situation where none of the other FBGs is perturbed, *equilibrium state*. During one wavelength sweep, only pulses at the individual FBG resonance wavelengths $\lambda_{B,k}, k = 1, ..., K$, will be reflected and received with a delay corresponding to the sweep rate and the FBG position. Variations in temperature or strain cause a shift of the resonance wavelength and, hence, affect the delay of the received signal. At high sweep rates, the wavelength evolves faster and is swept quickly through the resonance region of the FBGs resulting in a reflected signal of small temporal extension. The same holds for a smaller laser linewidth which can be achieved by providing higher dispersion in the laser cavity or by increasing f_m [3, 9]. Strongly confined reflections offer higher spatial resolution.

For the k-th FBG, the relative delay of the received signal with respect to the signal reflected at FBG$_j$ is given by

$$\Delta t_{(k,j)} = |\tau_k - \tau_j|, \quad k, j = 1, ..., K,\ k \neq j\ , \qquad (1)$$

where τ_k, τ_j are the total delays of the k-th and j-th FBG with respect to the trigger which is reset at the sweep rate. The system parameters, $\Delta t_{(k,j)}, \forall\, k, j$, are well known for the equilibrium state. When the resonance wavelength is shifted by a small value $\delta\lambda_k$ to $\lambda_{B,k} \pm \delta\lambda_k$ due to perturbations, the time delay varies according to $\widetilde{\Delta t}_{(k,j)} = |\tilde{\tau}_k - \tau_j| = |(\tau_k \pm \delta t_k) - \tau_j|$. Denoting the overall swept wavelength range by R_{sw} and the sweep rate by S_r, the shift of the reflected wavelength is related to the delay variation δt_k by [3, 9]

$$\delta\lambda_k = \delta t_k \cdot S_r \cdot R_{\text{sw}}\ . \qquad (2)$$

These delays are well characterized by comparing the the amplitude peaks of the reflected signal.

Finally, a slow photodiode (PD), unable to follow the fast pulses, is adopted to extract the pulse train envelope of the received signal [11] which is then gathered via CS-based acquisition as described in Section 4. One sweep corresponds to one CS-sample. If we denote the sweep duration $T_{\text{sw}} = 1/S_r$, the total delay of acquiring M CS-samples, in addition to a calculation time T_{cal} for subsequent signal reconstruction, becomes $T_{\text{up}} = M \cdot T_{\text{sw}} + T_{\text{cal}}$. The sensor measurements of the k-th FBG, $s_k(t), k = 1, ..., K$, show functional dependence on the perturbation of interest such as temperature or strain, and can be described in terms of the measured delay to the reference point (FBG$_j$) by

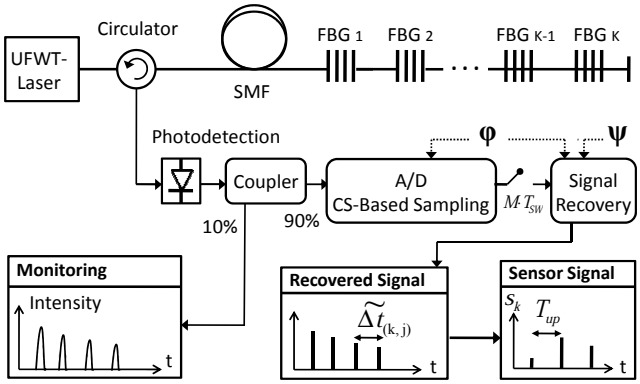

Fig. 1. System setup of a CS-based FBG sensor using a UFWT-class laser according to [3, 9].

$$s_k(T_n) = f_k(\widetilde{\Delta t}_{(k,j)})\ , \qquad (3)$$

where $T_n = n \cdot T_{\text{up}},\ n \in \mathbb{N}$, is the time instant when the n-th sensor measurement is available. The functions $f_k, k = 1, .., K$, depend on the specific characteristics of the FBGs and the type of perturbation. With all this information at hand, we arrive at an automated process for detecting and measuring impairments using CS-based FBG sensing systems.

3. SIGNAL MODEL

A comprehensive model for the reflected signal has to account for the laser class in use and all significant impairments the signal experiences during the sensing process such as fiber propagation, reflection at the FBGs and photodetection. We assume knowledge about the laser source, fiber length, dispersion parameters, as well as location and reflection properties of the single FBGs. The first and second order dispersion parameters of the fiber, $D(\lambda)$ and $S(\lambda)$, are derived from the Sellmeier equation at wavelength λ and with parameters given e.g. in [12]. Practically, they are determined by a three-/five-term Sellmeier fit to the measured group delay [13].

a) Laser Output Pulses:

The pulse shape of the emitted light for an actively mode-locked fiber laser in the baseband frequency domain can be described by chirped Gaussian pulses of the form [3, 9]

$$A^{(\lambda)}(\omega) = e^{-\frac{\omega^2}{2\delta\omega^2}}\ . \qquad (4)$$

with wavelength-dependent bandwidth

$$\delta\omega = \sqrt{\pi \frac{f_m}{\lambda}} \left(\frac{8\pi c_0 \Gamma}{|D(\lambda)| L_{\text{DCF}}} \right)\ . \qquad (5)$$

c_0 is the speed of light, Γ the modulation index for amplitude modulation of the light within the laser cavity, f_m is the modulation frequency of the SOA-modulating signal and L_{DCF} is

the length of the DCF (laser cavity) [3, 9]. During one sweep, the i-th pulse in the emitted pulse train is comprised of the superimposed modes around the instantaneous center wavelength λ_i. The pulse repetition rate in our model is the same as the modulation frequency (and varies accordingly), which is consensual with [3, 9]. The instantaneous delay between two subsequent pulses at index i is $\tau_{\text{rep},i} = \frac{1}{f_{m,i}}$. The temporal waveform consists of the sum of all pulses exhibited from the laser during one sweep. Its shape is determined by the wavelength-dependent gain profile of the SOA within R_{sw}.

b) SOA Gain Profile:

Signal amplification and the gain in the active region of the SOA can be derived from the photon- and carrier-density rate equations [14]. We use a 3rd-order model for the SOA gain profile and basis parameters from [14]:

$$g(\lambda) = a_1(N - N_0) - a_2(\lambda - \lambda_N)^2 + a_3(\lambda - \lambda_N)^3 \,. \quad (6)$$

a_{1-3} are empirical constants to fit the measured data, λ_N is the maximum gain wavelength and N, N_0 are carrier densities [14]. We fitted the model to achieve a 3dB bandwidth of 85.7 nm according to the reference system in [3, 9].

c) Fiber Transmittion:

The generated pulses at the laser output are now transmitted over a single-mode fiber (SMF) of length L to the location of an FBG. For small intensities, non-linear effects are negligible and we can find the baseband transfer function of the fiber of length L, including 2nd-order dispersion, by [15, 16]

$$H^{(\lambda)}(\omega, L) = e^{(-\alpha^{(\lambda)} + j\frac{\beta_2^{(\lambda)}}{2}\omega^2 + j\frac{\beta_3^{(\lambda)}}{6}\omega^3)L} \,, \quad (7)$$

in which $\alpha^{(\lambda)}$ is the damping as determined in [17], and $\beta_2^{(\lambda)}$, $\beta_3^{(\lambda)}$ are respectively the 1st- and 2nd-order terms in the Taylor expansion of the propagation constant $\beta(\omega)$. These are derived from $D(\lambda)$, $S(\lambda)$ according to [15] for the instantaneous center lasing wavelength λ_i of each pulse.

d) Bragg Grating Model:

An FBG can be modeled by a uniform, periodic perturbation of the refractive index along the fiber core in propagation (z-) direction as in [18]:

$$n(z) = n_0 + \Delta n \left(\frac{2\pi z}{\Lambda}\right) \,,\; z \in [0, L_{\text{FBG}}] \,, \quad (8)$$

where L_{FBG} is the total grating length, n_0 is the average refractive index within one spatial period Λ, and Δn is the perturbation amplitude. The effect of the grating on the signal is well described by the grating equation, from which the Bragg condition is derived that determines the wavelength of maximum reflectivity [18]. Based on this, the reflectivity for the electric field amplitude is found using coupled mode theory, i.e. [18, 19]

$$\rho(\lambda) = \frac{-\kappa \sinh(s\, L)}{\Delta\beta \sinh(s\, L) + i\, s \cosh(s\, L)} \,, \quad (9)$$

where $s = \sqrt{\kappa^2 - \Delta\beta^2}$, κ is the coupling coefficient and $\Delta\beta = \beta - \frac{\pi}{\Lambda}$ is a detuning wavevector for a mode with propagation constant β according to [18]. Since these parameters depend on the wavelength, $\rho(\lambda)$ depends implicitly on the wavelength as well.

e) Received Waveform at the Photodiode:

After reflection at the grating, the signal travels back the same way to the photodiode (PD) of the receiver. Thus, the fiber transfer function is applied twice. When the center frequency of the sweep range is $\Omega_0 = c_0/\lambda_0$, the optical frequency of the i-th pulse is $\Omega_i = \Omega_0 - \Delta\omega_i$, where $\Delta\omega_i = c_0 \left(\frac{1}{\lambda_0} - \frac{1}{\lambda_i}\right)$. Using equations (4,6,7,9), we obtain an expression in the frequency domain for the overall received signal pulse train, reflected at an FBG located at distance L in the fiber:

$$E_r(\omega) = \sum_i g_i\, \rho_i\, e^{-j\omega\tau_{\text{rep},i}} A_i(\omega - \Delta\omega_i)\, H_i(\omega - \Delta\omega_i)^2 \,. \quad (10)$$

Index i indicates the dependence of each element on λ_i. Taking the inverse Fourier transform of $E_r(\omega)$ results in the time-domain signal $E_r(t)$. The photodetection process, described by the responsitivity $R(\lambda)$ of the PD, depends on the quantum efficiency η of the material at λ_i [20] and distinct PD types require individual models. For simplicity, we assume the incident electric field and, hence, the intensity $I(\vec{r}, t)$ being uniformly distributed at all locations $\vec{r}$ on a photodetector with unit area $\tilde{A}$. Then, the incident power becomes $P(t) = \int_{\tilde{A}} I(\vec{r}, t) d\tilde{A} = \frac{1}{Z}|E_r(t)|^2$, where Z is the wave impedance of the medium [20]. At a sweep rate S_r, we denote the time-dependent wavelength by $\lambda(t)$, so the detected photocurrent is given by [20]

$$i(t) \;= R(\lambda(t)) \cdot P(t) = \frac{\lambda\, \eta\, q}{h\, c_0} \frac{|E_r(t)|^2}{Z} \,, \quad (11)$$

where h is Planck's constant and q is the elementary charge [20]. We deploy a slow photodiode that cannot follow the fast pulses to extract the pulse train envelope according to [11]. This can be modeled by a lowpass filter with transfer function $H_{\text{LP}}(\omega)$, i.e.

$$i_{\text{env}}(t) = \frac{1}{2\pi} \int_{-\infty}^{\infty} e^{j\omega t} \; [H_{\text{LP}}(\omega) \cdot i(\omega)] \; d\omega \,. \quad (12)$$

4. COMPRESSIVE FIBER SENSING

Any complex signal $\mathbf{r} \in \mathbb{C}^N$ can be represented by

$$\mathbf{r} = \mathbf{\Psi x}, \qquad \text{and} \qquad \mathbf{x} = \mathbf{\Psi}^H \mathbf{r} \;\in \mathbb{C}^N. \quad (13)$$

with basis matrix $\mathbf{\Psi} \in \mathbb{C}^{N \times N}$ and sparse coefficient vector $\mathbf{x}$ [10]. CS requires $\mathbf{r}$ to be K-sparse, meaning that $\mathbf{x}$ has only K non-zero entries [10]. Compared to Nyquist sampling, the number of acquired samples is strongly reduced since the observations are taken by $M \ll N$ random projections, i.e.

$$\mathbf{y} = \mathbf{\Phi r} = \mathbf{\Phi\Psi x} \;:=\; \mathbf{\Theta x} \quad \in \mathbb{C}^M \,. \quad (14)$$

The measurement matrix $\mathbf{\Phi} \in \mathbb{R}^{M \times N}$ has independent and identically distributed entries following a certain random distribution [10]. The signal can be reliably recovered by solving the underdetermined equation system in (14) using sparse optimization for which efficient solvers are available [10].

When the received signal of an FBG sensing system is sampled at the Nyquist rate with sampling period T_s, N samples of the pulse train envelope are collected, i.e. $r(n) = i_{\text{env}}(n\,T_s)$, $n = 0, ..., N-1$. In contrast, when using CS to acquire $M \ll N$ measurements (M wavelength sweeps), the average sampling rate is significantly reduced. The entries of $\mathbf{\Phi}$ can be chosen from the Database-Friendly distribution [21] which requires little storage owing to its sparse structure. Moreover, its high probability of zero-projection allows to reduce computational costs and required average sampling rate [21]. Basically, $\mathbf{\Phi}$ can be generated via pseudo-random sequences without static memory allocation using a fixed initialization. Also $\mathbf{\Psi}$ can be iteratively constructed from a view parameters. Thus, the total storage reduction is $\sim (N - M)$. As shown in Figure 2, the received signal based on our model is intrinsically sparse, so ideally $\mathbf{\Psi} = \mathrm{I}$ is the unity matrix and $\mathbf{r} = \mathbf{x}$. Then, the non-zero elements in $\mathbf{x}$ indicate the temporal positions and relative delays of the reflected signals. The number of FBGs in our system, K, is usually known and the number of appearing peaks in $\mathbf{x}$ can be controlled accordingly in the reconstruction algorithm, e.g. by limiting the number of iterations as presented in [22]. However, under non-ideal conditions in practical systems, the received signal may not exhibit a sparse range profile. In that case, it is possible to apply CS by selecting $\mathbf{\Psi}$ from a wavelet-basis, e.g. Symlets. As shown in Figure 3, a peak detection algorithm can subsequently determine the relative distance of the reflected signals for the single FBGs with respect to the reference point.

The perturbation at the FBGs and, hence, the coefficient vector $\mathbf{x}$ is assumed constant during the acquisition of M CS samples (M wavelength sweeps). Nevertheless, fast acquisition is achieved by exploiting the high sweep rate of UFWT-lasers which allows to follow moderately time-varying perturbations at the FBGs. Efficient dynamic updating schemes in the reconstruction algorithm further alleviate this constraint since the calculation time T_{cal} is reduced.

5. SIMULATIONS AND EXPERIMENTAL RESULTS

In this section, we show simulations of the analytical model from Section 3 and verify our proposed technique using experimental data taken from the system in [3, 9]. The Yamashita laboratory, University of Tokyo, Japan, kindly provided measurements for this purpose.

The left side of Fig. 2 depicts the train of short pulses ($\sim$ 1 ns) emitted by the UFWT laser during one sweep. It clearly follows the SOA gain profile and is in good agreement with the measurements in [3, 9]. In Fig. 2 (middle), the reflectivity spectrum of the FBG, according to our model, is compared to

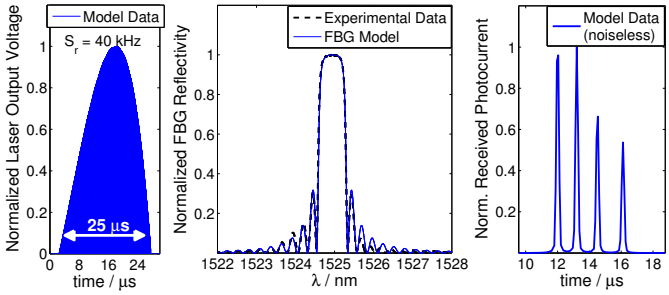

Fig. 2. Simulated laser output (left), FBG reflectivity (middle) and received signal reflected at 4 FBGs (right)

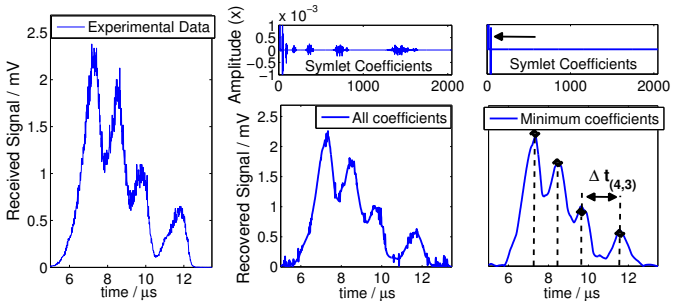

Fig. 3. CS-based fiber sensing using symlets and peak detection applied to experimental data taken from [3, 9]

the experimentally determined reflectivity of FBG_1 in [3, 9]. A proper fitting is achieved here as well. Finally, in Fig. 2 (right), we show $N = 112$ samples of the received photocurrent from (12), acquired at the Nyquist rate, and with $K = 4$ as in [3, 9]. After reconstruction, the relative peak delays indicate the amount of perturbation. Table 1 shows the detection rate and T_{cal} vs. the numbers of CS-samples averaged over 5000 Monte Carlo runs and with accuracy $\sim 0.6\,\mu$s. The experimental data in Figure 3 (left) shows broadening and overlap of the received signals which, to the belief of the authors in [3, 9], originates from an increased linewidth at high scan rates and from insufficient speed of the A/D converter. Thus, we adopted a wavelet basis (Symlets) for CS as mentioned in Section 4. Figure 3 (right) shows the reconstructed signal when either all or only the significant wavelet coefficients are used. We employed a homotopy-based solver as e.g. in [22].

# Meas. (out of N)	40	50	60	70	80	90
Det. Rate (in %)	53	62	70	76	80	85
T_{cal} (ms)	1.5	1.9	2.3	3.5	7.1	7.2

Table 1. Peak detection and T_{cal} for different M

6. CONCLUSION

We presented a sparse acquisition scheme for FBG sensing using UFWT-class lasers as proposed in [3, 9]. Their combined advantages are: reduced hardware costs (no tunable filters), high sweep rates for dynamic sensing which is also advantageous for CS, as well as reduced storage requirements

and abated average sampling rate. The latter has potential to further reduce hardware costs, replacing costly high-speed A/D converters. Our proposed CS-scheme uses the sparse range profile of the reflected signal for direct peak detection but it also works for non-sparse range profiles via wavelet bases. We further provided a comprehensive signal model that can be applied for FBG sensors based on UFWT-class lasers with arbitrary sensing structure. The application of our technique to dynamic sensing is currently under investigation and planned to be reported soon.

7. ACKNOWLDEGEMENTS

The authors wish to thank Professor Shinji Yamashita and his group from The University of Tokyo, 7-3-1 Hongo, Bunkyo-ku, Tokyo 113-8656, Japan, for kindly providing the experimental data of the FBG sensor system in [3, 9], and the Graduate School of Computational Engineering at Technische Universität Darmstadt for the support of this work.

8. REFERENCES

[1] A. Kersey, M. Davis, H. Patrick, M. LeBlanc, K. Koo, C. Askins, M. Putnam, and E. Friebele, "Fiber grating sensors," *J. Lightwave Technol.*, vol. 15, no. 8, pp. 1442 –1463, Aug. 1997.

[2] K. Hotate and Z. He, "Synthesis of optical-coherence function and its applications in distributed and multiplexed optical sensing," *J. Lightwave Technol.*, vol. 24, no. 7, p. 2541, July 2006.

[3] Y. Nakazaki and S. Yamashita, "Fast and wide tuning range wavelength-swept fiber laser based on dispersion tuning and its application to dynamic fbg sensing," *Opt. Express*, vol. 17, no. 10, pp. 8310–8318, May 2009.

[4] K. Hung, C. Lee, W. Chan, S.-O. Choy, and P. Kwok, "Development of novel wearable sensors for mobile health," in *IEEE-EMBS International Conference on Biomedical and Health Informatics (BHI)*, Jan. 2012, pp. 745 –747.

[5] A. Mendez, "Fiber bragg grating sensors: a market overview," *Proc. SPIE 6619, Third European Workshop on Optical Fibre Sensors, 661905, July 02, 2007*, vol. 6619, pp. 661 905–661 905–6, 2007.

[6] M. Iodice, V. Striano, G. Cappuccino, and G. Cocorullo, "Fiber bragg grating sensors-based system for strain measurements," in *Proceedings of 2005 IEEE/LEOS Workshop on Fibres and Optical Passive Components, 2005*, June 2005, pp. 307 – 312.

[7] K. Hill and G. Meltz, "Fiber bragg grating technology fundamentals and overview," *Journal of Lightwave Technology*, vol. 15, no. 8, pp. 1263 –1276, Aug. 1997.

[8] T. Amano, H. Hiro-Oka, D. Choi, H. Furukawa, F. Kano, M. Takeda, M. Nakanishi, K. Shimizu, and K. Ohbayashi, "Optical frequency-domain reflectometry with a rapid wavelength-scanning superstructure-grating distributed bragg reflector laser," *Appl. Opt.*, vol. 44, no. 5, pp. 808–816, Feb. 2005.

[9] S. Yamashita, Y. Nakazaki, R. Konishi, and O. Kusakari, "Wide and fast wavelength-swept fiber laser based on dispersion tuning for dynamic sensing," *Journal of Sensors*, vol. 2009, p. 12, 2009.

[10] R. G. Baraniuk, "Compressive sensing [lecture notes]," *IEEE Signal Processing Magazine*, vol. 24, pp. 118 – 121, 2007.

[11] F. Salin, P. Grangier, P. Georges, G. L. Saux, and A. Brun, "Nonreciprocal phase shifts in a femtosecond dye laser," *Opt. Lett.*, vol. 15, no. 16, pp. 906–908, 1990.

[12] B. E. A. Saleh and M. C. Teich, *Grundlagen der Photonik*. Wiley, 2008.

[13] B. P. Pal, *Fundamentals Of Fibre Optics In Telecommunication And Sensor Systems*. New Age International Publishers, 2005.

[14] A. Willner and W. Shieh, "Optimal spectral and power parameters for all-optical wavelength shifting: single stage, fanout, and cascadability," *Journal of Lightwave Technology*, vol. 13, no. 5, pp. 771 –781, May 1995.

[15] M. Seimetz, *High-Order Modulation for Optical Fiber Transmission: Phase and Quadrature Amplitude Modulation*. Springer, 2009.

[16] E. Ip, A. P. T. Lau, D. J. F. Barros, and J. M. Kahn, "Coherent detection in optical fiber systems," *Opt. Express*, vol. 16, no. 2, pp. 753–791, Jan. 2008.

[17] E. Voges and K. Petermann, *Optische Kommunikationstechnik*. Springer, 2002.

[18] H. Venghaus, Ed., *Wavelength Filters in Fibre Optics*. Springer, 2006.

[19] R. Kashyap, *Fiber Bragg Gratings*. A. P., 2009.

[20] S. B. Alexander, *Optical Communication Receiver Design*. SPIE Publications, 1997.

[21] D. Achlioptas, "Database-friendly random projections: Johnson-lindenstrauss with binary coins," *J. Computer and System Sciences*, vol. 66, no. 4, pp. 671–687, 2003.

[22] D. M. Ujdat, D. M. Malioutov, M. Cetin, and A. S. Willsky, "Homotopy continuation for sparse signal representation," in *In Procedings IEEE International Conference on Acoustics, Speech, and Signal Processing*, 2005, pp. 733–736.